Nanotechnology **21** (2010) 225705 (7pp) doi:10.1088/0957-4484/21/22/225705

High-speed atomic force microscopy for large scan sizes using small cantilevers

Christoph Braunsmann and Tilman E Schäffer

Institute of Applied Physics, University of Erlangen-Nuremberg, Staudtstraße 7, Building A3, 91058 Erlangen, Germany

E-mail: schaeffer@physik.uni-erlangen.de

Received 2 January 2010, in final form 31 March 2010
Published 7 May 2010
Online at stacks.iop.org/Nano/21/225705

Abstract

We present a high-speed atomic force microscope that exhibits a number of practical advantages over previous designs. Its central component is a high-speed scanner with a maximum scan size of 23 μm × 23 μm and a conveniently large sample stage area (6.5 mm × 6.5 mm). In combination with small cantilevers, image rates of up to 46 images s^{-1} in air and 13 images s^{-1} in liquid are reached under z-feedback control. By large scan size imaging of collagen fibrils in air, sample velocities of 8.8 mm s^{-1} in the xy-direction and 11 mm s^{-1} in the z-direction are reached. To provide optimized imaging conditions for both large and small scan sizes, a modular scanner design allows easily exchanging the x- and y-piezos. The scanner is therefore also suited for investigations on the molecular and atomic scale, which is demonstrated by imaging the step dynamics of a calcite surface during dissolution and the hexagonal lattice of a mica surface in liquid.

S Online supplementary data available from stacks.iop.org/Nano/21/225705/mmedia

(Some figures in this article are in colour only in the electronic version)

1. Introduction

Since its invention by Binnig *et al* in 1986 [1], the atomic force microscope (AFM) has proven to be a powerful instrument for the study of surfaces on the nanoscale. Investigations can be done in vacuum, air or liquid environments and therefore the applications range from semiconductor physics to life science. By using conventional AFMs, surfaces can be imaged with typical line rates between 0.1 and 10 Hz, resulting in acquisition times of several minutes per image. A higher imaging rate is desirable, because this increases the data throughput of the microscope [2] and broadens the field of application to the investigation of dynamic processes that occur on shorter timescales [3]. Up to 1000× higher scan speeds are possible by consequently increasing the bandwidth of every single electronic (detector electronics, feedback controller, piezo amplifier, etc) and mechanical AFM component (cantilever, scanner, etc) [4]. Increasing the bandwidth of the AFM scanner is particularly difficult. Especially the z-scanner needs to react fast for a high-speed, feedback-controlled system.

First work towards high-speed AFM was done by Barret and Quate, who imaged the surface of a metal–semiconductor field-effect transistor with a scan size of 8 μm × 8 μm and a line rate of 600 Hz (≈3 images s^{-1}) in constant-height contact mode (without z-feedback control) [2]. Soft samples, however, were damaged by the varying imaging force during high-speed scanning. To overcome this problem, cantilevers with integrated piezo actuators were developed that could react to height variations much faster than the previously used tube scanner [5]. Constant-force images of integrated circuits were recorded in air with a sample velocity of 3 mm s^{-1} in the xy-direction. The xy-scanning motion was generated by a tube scanner, driven at a 50 Hz line rate and a scan size of 30 μm × 30 μm, with a sinusoidal waveform.

The group of Hansma introduced the concept of small cantilevers for high-speed imaging in 1996 [6]. They showed that cantilevers ≈10× smaller than conventional ones have higher resonant frequencies and lead to higher imaging speeds, while still providing small spring constants needed for gentle imaging of soft samples. As these cantilevers do not work in conventional AFMs, they designed an optical beam deflection detector for small cantilevers, featuring a small focused optical spot size [7, 8]. Furthermore, they developed a rigid xyz-scanner with a maximum scan size of 13 μm × 13 μm

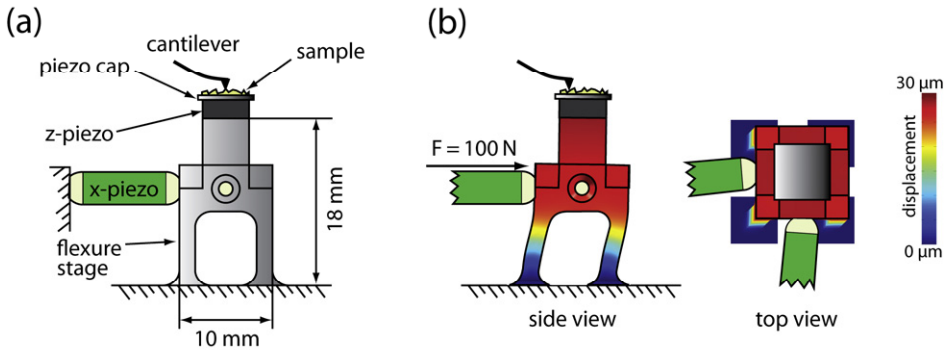

Figure 1. (a) Schematic diagram of the high-speed scanner (side view). The x-piezo and the y-piezo (out of the image plane, not drawn) push against the flexure stage made out of aluminum. The z-piezo is glued on top of the stage. The sample is fixed onto the piezo cap by vacuum grease or glue. (b) Displacement of the flexure stage under a preload force of 100 N in the x- and y-direction, calculated by finite element modeling (drawn 50× exaggerated). The color of the flexure stage indicates the total displacement relative to the unloaded stage.

and acquired constant-force contact mode images of a silicon calibration grating with a line rate of up to 2060 Hz and a scan size of ≈8 μm × 8 μm [9, 10].

The group of Ando developed several high-speed electronic components, a setup for small cantilevers and high-speed scanners with scan sizes of up to 4.5 μm × 4.5 μm [4, 11]. Several biomolecular processes were imaged in amplitude modulation mode in liquid with recording times of down to 30–60 ms/image for a scan size of ≈250 nm × 250 nm. Fukuma *et al* recently presented a novel inertia balance support method for high-speed scanning [12].

A video-rate control system for scanning probe microscopes was introduced by Rost *et al* in 2005 [13]. They showed movies of a highly-ordered pyrolytic graphite (HOPG) surface taken with scanning tunneling microscopy with a rate of 80 images s^{-1} (128 pixels × 128 pixels) and a scan size of a few nanometers. The scan sizes of their other high-speed images were up to 240 nm, with line rates of 586 Hz and sample velocities of 0.3 mm s^{-1}. However, high-speed imaging with AFM was not demonstrated.

A different approach was explored by the group of Miles. They developed scanners for scanning near field optical microscopy [14] and for atomic force microscopy [15] which use the mechanical resonance of a tuning-fork for scanning either the probe or the sample with line rates of ≈20 kHz in the fast scan direction. Constant-height images of poly(ethylene-oxide) crystals with a recording time of 14.3 ms and a scan size of ≈4 μm × 4 μm were presented. During these measurements the tip reached enormous velocities of up to 22.4 cm s^{-1} relative to the sample. Using a resonant scanner, Zhao *et al* imaged a silicon calibration grid in air with a large scan size of 37.5 μm × 37.5 μm and a (resonant) line frequency of 772 Hz [16]. While these numbers are impressive, there are a number of disadvantages of this approach. For example, it only works in the constant-height mode. It is therefore not possible, due to lacking z-feedback, to control the force acting on the sample during imaging on a pixel-by-pixel basis. Furthermore, the line rate of these resonant scanners cannot easily be changed.

In this paper we present the design and applications of a high-speed AFM for small cantilevers. A novel flexure-based xyz-scanner with a large sample stage and a large scan size of 23 μm × 23 μm achieves line rates in the kilohertz range. A fast z-feedback control allows gentle imaging of soft samples in air and in liquid. The x- and y-piezos are easily exchangeable, allowing us to choose piezos with optimum properties for a given scan size. Therefore, the new scanner can be applied to a large variety of different samples and thus has a broad range of applications.

2. Experimental methods

2.1. Mechanical scanner design

The high-speed scanner is based on a small aluminum flexure stage with a width of 10 mm and a height of 18 mm (figure 1(a)). The xy-scanning motion is realized by two piezoelectric actuators (xy-piezos) which are preloaded against the flexure stage. The complete stage elastically follows the forward and backward motion of the xy-piezos, which are driven by the xy-scan-voltages. For moving the sample in the z-direction a z-piezo is glued on top of the stage. It is covered by a thin piezo cap made out of aluminum. The sample is attached to the piezo cap by the use of vacuum grease or glue. The flexure stage is enclosed in silicon rubber for passive damping (not shown in figure 1).

The xy-piezo stacks are terminated with spherical end pieces made of corundum. Adjustment screws (not shown in figure 1) apply the preload that pushes the piezos against the stage. This adjustable preloading mechanism has two advantages. First, it allows changing the sample position relative to that of the cantilever by slightly varying the preload. Second, it allows quickly exchanging the piezos, because the piezos are not glued in. In our current setup we use two alternative piezo sizes: 7 mm stack height for small scans with high lateral resolution and 20 mm stack height for large scans (Piezomechanik GmbH, München, Germany). These piezos allow a maximum scan size of 10 μm × 10 μm and 23 μm × 23 μm, respectively. Even smaller or larger piezos can easily be used, too.

As z-piezo, we use a 2 mm high piezo stack (Physik Instrumente GmbH, Karlsruhe, Germany). This piezo has

a nominal fundamental resonant frequency of ≈150 kHz if clamped at one side and is therefore well-suited for a high-speed scanner. Having a cross-section of 5 mm × 5 mm it allows attaching a sample stage (the piezo cap) with a cross-section of about 6.5 mm × 6.5 mm. The maximum z-displacement is 3.3 μm.

2.2. Static properties

Figure 1(b) illustrates the simulated displacement of the flexure stage under a preload force of 100 N each in the x- and y-direction. This simulation was done by finite element modeling (COMSOL Multiphysics 3.5, COMSOL AB, Stockholm, Sweden). The color indicates the total displacement of the stage relative to that at 0 N preload. The drawn deformation is exaggerated by a factor of 50. If a piezo with a stiffness k_{piezo} acts against a mechanical system with a stiffness k_{mech}, its maximum free displacement ΔL_0 is reduced to $\Delta L \approx \Delta L_0 k_{\mathrm{piezo}}/(k_{\mathrm{piezo}} + k_{\mathrm{mech}})$. The transversal spring constant of the flexure stage was calculated as 5.1 N μm^{-1}. With a piezo-stiffness of ≈60 N μm^{-1} the maximum xy-displacement is thus reduced by only ≈10%.

Finite element modeling was also used for investigating the amount of cross coupling between the different axes of motion. We found that the coupling increases with the magnitude of the preload, because preloading slightly deforms the flexure stage (figure 1(b)). The deformation has two effects. First, the actual scan directions of the x- and y-piezos deviate from the x- or y-axis, respectively, leading to a coupling between the x- and y-direction ('xy-coupling'). Second, the sample stage becomes tilted relative to the xy-plane, leading to a coupling between the xy-scan-directions and the z-direction ('xy–z-coupling'). But the deformation and thus the coupling can be kept small. A preload of 100 N is more than sufficient to protect the xy-piezos against tensile forces, which do not exceed 1 N even for a line rate of 1 kHz and a piezo displacement of 23 μm. For a 100 N preload force in the x- and y-direction each and an x-displacement of 23 μm we calculated that a sample will move ≈2.7 nm in y and ≈15 nm in z. As a conclusion, the xy-coupling is negligible and the xy–z-coupling (<0.07%) is only relevant for flat samples at large scan sizes and can easily be corrected by a planar fit.

2.3. Dynamic properties

The maximum scan speed of the scanner is limited by its mechanical resonances. Lateral resonances (oscillations in the xy-plane) can be excited by high-frequency scanning motions and thus set an upper limit to the usable line rates. Longitudinal resonances (oscillations in the z-direction) narrow the bandwidth of the z-feedback loop because at such resonances the z-piezo usually responds with a high gain and a large phase lag, and thus the feedback control becomes instable [5]. This may result in large imaging forces, which can damage the tip or sample. Therefore, both the lateral and the longitudinal resonant frequencies should be as large as possible. (We note that for complex mechanical systems, a distinct separation between lateral and longitudinal resonances can be difficult or impossible, because of a coupling between the different axes of motion. We will therefore use the terms 'predominantly lateral' and 'predominantly longitudinal' in the following.)

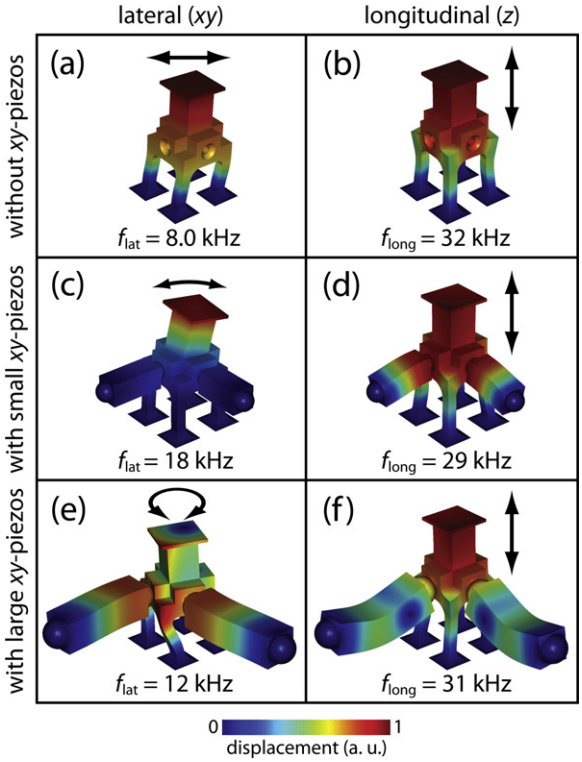

Figure 2. First predominantly lateral (left column) and first predominantly longitudinal (right column) resonances of the high-speed scanner calculated by finite element modeling. Due to the modular design, three different finite element models were developed. (a) and (b) show the resonances of a model without xy-piezos. In (c) and (d) small xy-piezos were added. (e) and (f) show resonances of a model with large xy-piezos. It can be seen that the first (predominantly) longitudinal resonant frequency does not significantly depend on the presence or on the size of the xy-piezos.

Finite element modeling was used for optimizing the scanner design towards high resonant frequencies. Since the xy-piezos are exchangeable the scanner was modeled in three configurations: without xy-piezos (figures 2(a) and (b)), with small xy-piezos (figures 2(c) and (d)) and with large xy-piezos (figures 2(e) and (f)). The first mode of each model (left-hand column in figure 2) always occurs mainly in the xy-plane and can thus be classified as a predominantly lateral resonance. The mode shapes and the resonant frequencies considerably differ from each other due to the changed model geometry. Without the xy-piezos the entire flexure stage oscillates in the xy-plane with a frequency of 8 kHz (figure 2(a)). With small xy-piezos only the upper part of the flexure stage oscillates, with a frequency of 18 kHz, because the stage is supported by the piezos (figure 2(c)). In the case of large xy-piezos the first normal mode is a torsional oscillation at 12 kHz (figure 2(e)). For a triangular xy-scanning motion the maximum practical line rate is about a tenth of the first lateral resonant frequency (1.2–1.8 kHz). Higher line rates of up to ≈6 kHz become possible by using rounded triangular or

sinusoidal scanning motions. The fast and slow scan directions (x and y, respectively) can easily be swapped without lowering the maximum practical line rate, because the scanner design is symmetric in xy. This allows using the full range of scan angles.

The right-hand column in figure 2 shows the first predominantly longitudinal resonance of each model. The deformation of the flexure stage is almost identical for the three models and the corresponding resonant frequencies vary only slightly (in between 29 and 32 kHz). This implies that the boundary conditions relevant for the first longitudinal resonance are not significantly changed by these two types of xy-piezos. In particular, the bandwidth of the z-feedback loop needed for constant-force imaging is not reduced when using the large xy-piezos.

The additional mass of the piezo cap had little influence on the normal modes: removing the cap in the model resulted in ≈3% higher frequencies.

2.4. Other system components

Besides the scanner, several other components of our system were improved with respect to high speed. The optical lens system of the AFM head produces a laser spot size of 2.5 μm × 8.5 μm, compatible with the use of small cantilevers. The detector electronics, including the differential amplifier for calculating the deflection voltage, and the analog PID controller electronics have a bandwidth exceeding 1 MHz. The piezos are driven by a home-built high-voltage amplifier and the AFM is controlled by a home-built high-speed data acquisition system.

3. Results and discussion

3.1. Open and closed loop frequency response

To characterize the performance of the new scanner, we measured its open and closed loop frequency response in the z-direction by the use of a network analyzer (Hewlett Packard 4195A). For the open loop measurement the drive voltage of the z-piezo was modulated by connecting the output of the network analyzer with the input of the piezo amplifier. The resulting z-displacement was measured by recording the deflection of a cantilever that was in contact with the surface of the piezo cap. For the closed loop measurement, PID feedback control between the deflection and the drive voltage for the z-piezo was activated and the setpoint was modulated. An ARROW-UHF cantilever (NanoWorld, Neuchâtel) with a fundamental resonant frequency of 1.5 MHz, far beyond the first scanner resonances, was used.

Figure 3 shows the resulting Bode plots for a measurement with large xy-piezos (magnitude normalized to 0 dB at 1 kHz). The first slightly more pronounced peak in the open loop response (figure 3(a), solid line) occurs at 35 kHz and has a height of 1.6 dB. We attribute this peak to the first longitudinal resonance of the flexure stage shown in figure 2(f), which was calculated at a similar frequency (31 kHz). At this resonance the z-piezo responds with a phase shift of ≈−50° (figure 3(b), solid line). However, the peaks in figure 3(a) have a low gain, i.e. the open loop response shows a highly damped behavior

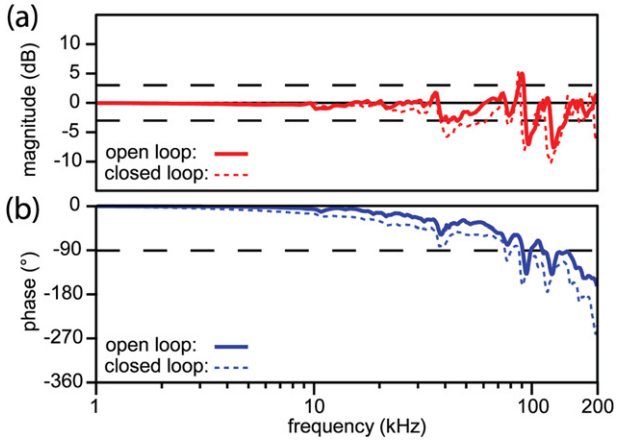

Figure 3. Bode plots showing the measured open loop (solid lines) and closed loop (dashed lines) frequency response of the high-speed scanner in the z-direction with large xy-piezos. (a) The first lateral resonance at 12 kHz (figure 2(e)) does not show in the magnitude of the open loop response and is thus not relevant for the speed of the z-feedback. The first pronounced peak occurs at 35 kHz and corresponds to the first longitudinal resonance shown in figure 2(f). The resonances have a low gain: the open loop magnitude stays within ±3 dB (dashed horizontal lines) up to ≈ 83 kHz. The closed loop response is almost identical to the open loop response. (b) Corresponding phase signals. The phase shift of the closed loop response stays above −90° up to ≈75 kHz.

and stays within a ±3 dB limit up to a frequency of ≈83 kHz. High damping is crucial for a fast step response with little overshoot and a short settling time.

Predominantly lateral resonances such as the one shown in figure 2(e) cannot be seen in figure 3, because their coupling with the z-direction is too small. As a consequence, these resonances do not affect the bandwidth of the z-feedback loop.

The closed loop response is shown by the dashed lines in figure 3. As expected, the PID feedback properly controls the deflection until the modulation frequency reaches the first predominantly longitudinal resonance (35 kHz). However, the closed loop phase shift stays above −90° up to a frequency of ≈75 kHz. The speed of a feedback loop is limited by the speed of the slowest component within the loop. In scanning probe microscopy the z-scanner usually is the slowest and most difficult to optimize component within the z-feedback loop [9]. This is the case also for our high-speed AFM, where the z-scanner and not the other components (section 2.4) limits the closed loop bandwidth.

The Bode plots for the scanner without or with small xy-piezos look essentially the same as the one for the scanner with large xy-piezos (as shown in figure 3). In particular, the frequency responses stay constant up to 31 kHz for the scanner without xy-piezos and up to 33 kHz for the scanner with small xy-piezos. As already mentioned in section 2.3 this shows again that the z-feedback bandwidth is not significantly influenced by the xy-piezos.

3.2. Collagen fibrils in air

In order to demonstrate the large scan size of our high-speed AFM we imaged type-I collagen fibrils prepared from rat tail

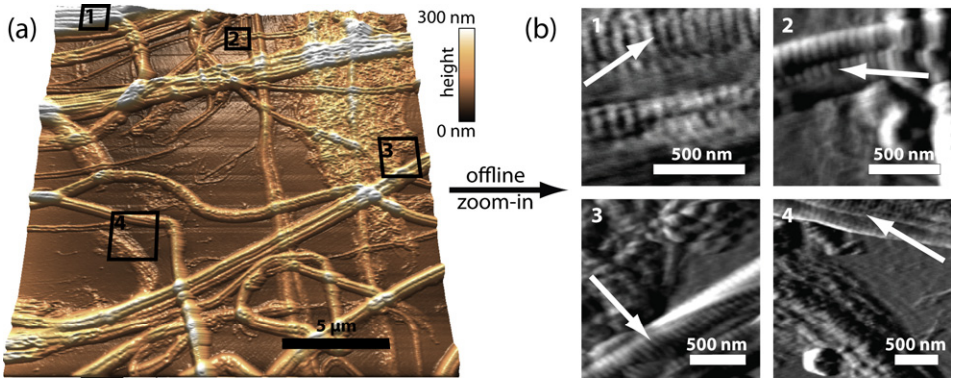

Figure 4. High speed, high resolution and large scan size imaging of collagen fibrils. (a) Topography image taken in contact mode in air with a line rate of 210 Hz and a scan size of 21 μm × 21 μm, resulting in a sample velocity of 8.8 mm s^{-1} in the xy-direction. 2000 lines were recorded per image with 2000 pixels each. A small Si_3N_4 cantilever, 20 μm in length, 2.5 μm in width, and 0.5 μm in thickness with a resonant frequency of 2.2 MHz was used (NanoWorld prototype cantilever). (b) Offline zoom-ins into the numbered boxes in (a). The high pixel density in (a) allows zooming offline into small parts of the image that show features of interest. The cantilever deflection and not the topography is displayed here for increased contrast. The 67 nm banding, which is characteristic for fibrillar type-I collagen, is clearly visible in all four images (arrows). The time that it would take to record images 1–4 separately would be 55 ms, 135 ms, 240 ms and 400 ms, respectively. The images are unprocessed except for slope removal.

tendons in contact mode in air with a line rate of 210 Hz and a xy-scan size of 21 μm × 21 μm (figure 4(a)). Single collagen fibrils appear with a height of 35–80 nm. The height of fibril bundles is up to 220 nm. Despite the high imaging speed, the z-feedback was fast enough so that the tip tracked the sample topography accurately. We showed this by imaging the same area with a line rate of only 5 Hz, resulting in identical fibril heights (data not shown).

At first glance a line rate of 210 Hz does not seem to match up with the line rates of more than 1 kHz reported by other groups. But together with the large 21 μm scan size this line rate results in an impressive sample velocity of 8.8 mm s^{-1} in the xy-direction. The maximum velocity in the z-direction is 11 mm s^{-1}, which we obtained by differentiating the topography image. We note that velocities (in the xy- and in the z-direction) rather than line or image rates are much more representative quantities for comparing the speed of different (feedback-controlled) high-speed scanners.

Figure 4(a) was recorded with a high resolution of 2000 pixels × 2000 pixels (=4 megapixels; the size of a typical CCD camera image). In many cases it is desirable to have one contiguous image of a large sample area with a high pixel resolution. In the past, researchers needed to take significant efforts to generate a high resolution image of a large, contiguous sample area by acquiring many neighboring images and stitching them together using image processing [17]. Such a procedure is not necessary for our scanner.

The high resolution allows us to zoom (offline) into small parts of the image that contain features of interest while maintaining a decent resolution. Figure 4(b) shows four zoom-ins into the numbered boxes in figure 4(a). The corresponding deflection and not the topography is shown, due to a better contrast. The 67 nm banding, which is characteristic for type-I collagen, can clearly be identified in all four images (arrows).

The acquisition time for the image shown in figure 4(a) was 9.5 s. This is ≈200× faster than what would have been possible with a conventional AFM with a line rate of ≈1 Hz,

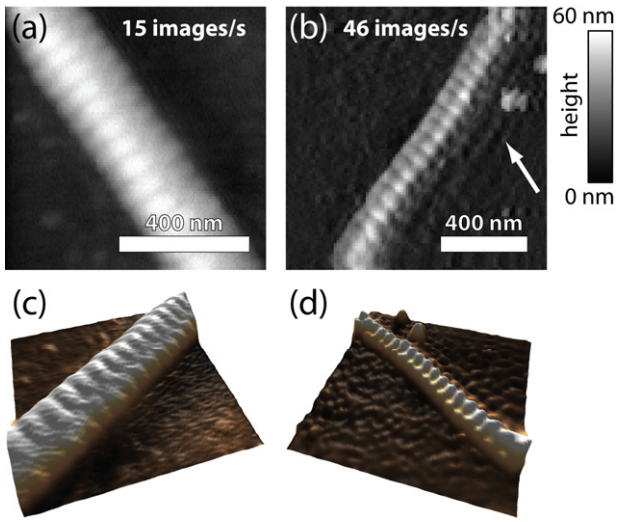

Figure 5. Ultra-high-speed topography imaging of different collagen fibrils in contact mode in air. (a) 15 images s^{-1}. The image was recorded with 100 lines of 200 pixels each, resulting in a line rate of 1.5 kHz. The scan size was 800 nm × 800 nm and the sample velocity ≈2.4 mm s^{-1} in the xy-direction. The 67 nm banding is clearly visible. (b) 46 images s^{-1}. The image was recorded with 100 lines of 100 pixels each resulting in a line rate of 4.6 kHz. The scan size was 1.2 μm × 1.2 μm and the sample velocity ≈11 mm s^{-1} in the xy-direction. The 67 nm banding is still visible, but the z-feedback shows a certain amount of ringing, especially behind the fibril (arrow). ((c), (d)) 3D-rendered data of (a) and (b), respectively.

where the same image would have taken about ≈0.5 h to acquire. Considering the areas of the four zoom-ins in (b) relative to the 21 μm × 21 μm scan area allows calculating the times that it would have taken to record the zoom-ins separately. This leads to effective acquisition times of only 55 ms, 135 ms, 240 ms and 400 ms, respectively.

In order to demonstrate that high image or line rates are also possible, we reduced the scan size to 800 nm × 800 nm and the pixel density to 100 pixels × 200 pixels.

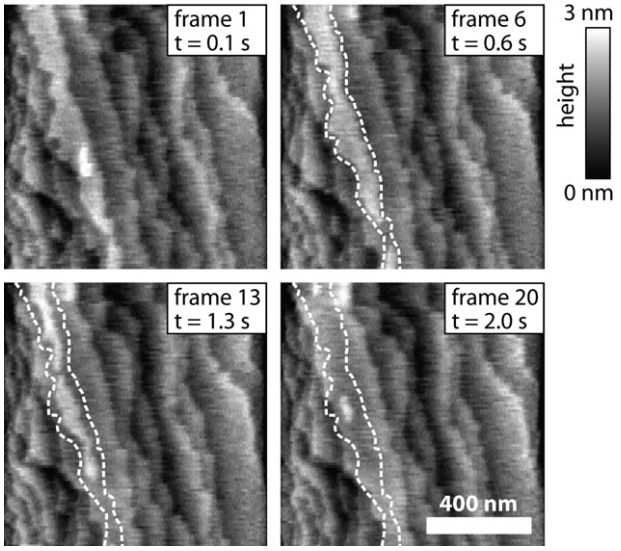

Figure 6. Dissolution of a calcite crystal in diluted hydrochloric acid. The topography image sequence was taken in contact mode in liquid with a rate of 10 images s^{-1}. The scan size was 1 μm × 1 μm and 100 lines of 400 pixels each were recorded, resulting in a line rate of 1.0 kHz. A small silicon cantilever, 18 μm in length, 4.5 μm in width and 0.5 μm in thickness was used. It had a resonant frequency of 1.1 MHz in air, 440 kHz in water and a spring constant of 1.0 N m^{-1} (NanoWorld prototype cantilever). The dissolution occurs mainly along the edges of the 3 Å high molecular layers, because here the crystal ions are less strongly bound. The dashed lines in frames 6, 13 and 20 mark the former boundary of the upper calcite layer from frame 1. The images are unprocessed except for slope removal. A movie of this sequence (supplementary movie 1 available at stacks.iop.org/Nano/21/225705/mmedia) and of a similar sequence that was taken with a rate of 13 images s^{-1} can be downloaded from the journal's homepage.

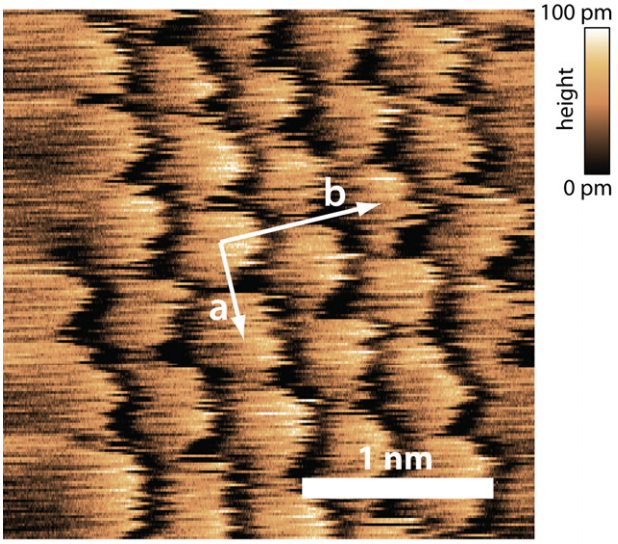

Figure 7. Atomic stick–slip effect on the muscovite mica {001} cleavage plane. The image was taken in contact mode in water. The scan size was 2.8 nm × 2.8 nm and 200 lines of 450 pixels each were recorded with a line rate of 63 Hz. A small Si_3N_4 cantilever, 20 μm in length, 7.5 μm in width and 0.5 μm in thickness was used. It had a resonant frequency of 641 kHz in air, 322 kHz in water and a spring constant of 0.7 N m^{-1} (NanoWorld prototype cantilever). The six-fold symmetry resulting from the hexagonal arrangement of SiO_4 tetrahedrons in the cleavage plane is clearly visible ($a \approx 5.2$ Å, $b \approx 9.0$ Å). The image shows that the high-speed scanner is not only suited for high-speed imaging with large scan sizes, but can also give molecular lattice resolution. The image is unprocessed except for slope removal.

This allowed us to record images of single collagen fibrils with a rate of up to 46 images s^{-1} (figure 5). The fibrils clearly show the characteristic 67 nm banding pattern in their topography. The line rates were 1.5 kHz (figure 5(a)) and 4.6 kHz (figure 5(b)). These line rates are about 100–1000× larger than those possible with conventional AFMs.

To increase the image quality without sacrificing scan speed, the images may be acquired with a larger number of points per line than number of lines per image (figures 5(a), (c), 6 and 7). This leads to rectangular pixels instead of square pixels in the displayed images.

3.3. Dissolution of a calcite crystal in diluted HCl

We further imaged the dissolution of a calcite crystal at the $\{10\bar{1}4\}$ cleavage face in contact mode in liquid. In water the dissolution is slow and stops when the water becomes saturated with calcium carbonate. Therefore, we injected hydrochloric acid into the fluid cell of the AFM head to speed up the dissolution. After the injection the HCl-concentration above the calcite surface was estimated as ≈0.02%. Figure 6 shows four topography images from a sequence acquired with a rate of 10 images s^{-1} (sample velocity: 2 mm s^{-1} in the xy-direction) (supplementary movie 1 available at stacks.iop.org/Nano/21/225705/mmedia). Several calcite monolayers with a step height of ≈3 Å are visible. The dissolution of the crystal occurs predominantly along the steps, where the crystal ions are less rigidly bound to the lattice. Measuring the spatial propagation of the steps as a function of time yielded an average step advancement rate of 22 ± 7 nm s^{-1}. A similar image sequence was acquired with a rate of 13 images s^{-1} (supplementary movie 2 available at stacks.iop.org/Nano/21/225705/mmedia).

Fast acquisition of image sequences is fundamental to the study of dynamic processes and is one of the main areas of application for high-speed AFM. Paired with the ability to image in liquid environments high-speed AFM has already contributed to the investigation of biomineralization [18], the movement of motor proteins [4] and DNA–protein-interactions [19].

3.4. Atomic stick–slip effect on muscovite mica

Figure 7 shows the height image of a muscovite mica {001} cleavage plane, recorded in contact mode in water with a small cantilever. The cleavage plane of muscovite consists of hexagonally arranged SiO_4 and AlO_4^- tetrahedrons distributed with a ratio of 3 to 1, respectively [20]. The corresponding six-fold symmetry can clearly be identified in figure 7. The contrast in the height image is caused by the atomic stick–slip effect that is well known from friction force microscopy rather than by the real topography of the top layer [21]. For this measurement we used the small xy-piezos (see section 2). This

result shows that our high-speed AFM is not only suited for high-speed, large scan size imaging but can also give molecular lattice resolution.

4. Conclusions

We designed a high-speed AFM for imaging with large scan sizes of up to 23 μm $\times$ 23 μm. This is the largest scan size for a feedback-controlled, high-speed xyz scanner reported to date. Sample velocities of 8.8 mm s^{-1} in the xy-direction and 11 mm s^{-1} in the z-direction were reached in contact mode imaging with small cantilevers, as was demonstrated by large scan size imaging of a collagen sample. Imaging rates of up to 46 images s^{-1} were presented. As an example for the investigation of fast dynamic processes in liquids, we imaged the dissolution of a calcite crystal in diluted hydrochloric acid with a rate of 13 images s^{-1}. Due to the modular design of the high-speed scanner, the xy-piezos can easily be exchanged. Small piezos can therefore be chosen for atomic resolution imaging, demonstrated by imaging the hexagonal lattice of a mica surface in water with a small cantilever.

Acknowledgments

We thank Johannes Rheinlaender and Yasuhiro Sugawara for discussions and NanoWorld for support.

References

[1] Binnig G, Quate C F and Gerber C 1986 *Phys. Rev. Lett.* **56** 930
[2] Barrett R C and Quate C F 1991 *J. Vac. Sci. Technol.* B **9** 302
[3] Drake B, Prater C B, Weisenhorn A L, Gould S A, Albrecht T R, Quate C F, Cannell D S, Hansma H G and Hansma P K 1989 *Science* **243** 1586
[4] Ando T, Kodera N, Takai E, Maruyama D, Saito K and Toda A 2001 *Proc. Natl Acad. Sci. USA* **98** 12468
[5] Manalis S R, Minne S C and Quate C F 1996 *Appl. Phys. Lett.* **68** 871
[6] Walters D A, Cleveland J P, Thomson N H, Hansma P K, Wendman M A, Gurley G and Elings V 1996 *Rev. Sci. Instrum.* **67** 3583
[7] Schäffer T E, Cleveland J P, Ohnesorge F, Walters D A and Hansma P K 1996 *J. Appl. Phys.* **80** 3622
[8] Schäffer T E and Hansma P K 1998 *J. Appl. Phys.* **84** 4661
[9] Kindt J H, Fantner G E, Cutroni J A and Hansma P K 2004 *Ultramicroscopy* **100** 259
[10] Schitter G, Åström K J, DeMartini B E, Thurner P J, Turner K L and Hansma P K 2007 *IEEE Trans. Control Syst. Technol.* **15** 906
[11] Ando T, Uchihashi T, Kodera N, Yamamoto D, Miyagi A, Taniguchi M and Yamashita H 2008 *Pflug. Arch.-Eur. J. Physiol.* **456** 211
[12] Fukuma T, Okazaki Y, Kodera N, Uchihashi T and Ando T 2008 *Appl. Phys. Lett.* **92** 243119
[13] Rost M J *et al* 2005 *Rev. Sci. Instrum.* **76** 053710
[14] Humphris A D L, Hobbs J K and Miles M J 2003 *Appl. Phys. Lett.* **83** 6
[15] Humphris A D L, Miles M J and Hobbs J K 2005 *Appl. Phys. Lett.* **86** 034106
[16] Zhao B, Howard-Knight J P, Humphris A D L, Kailas L, Ratcliffe E C, Foster S J and Hobbs J K 2009 *Rev. Sci. Instrum.* **80** 093707
[17] Picco L M, Bozec L, Ulcinas A, Engledew D J, Antognozzi M, Horton M A and Miles M J 2007 *Nanotechnology* **18** 044030
[18] Paloczi G T, Smith B L, Hansma P K, Walters D A and Wendman M A 1998 *Appl. Phys. Lett.* **73** 1658
[19] Crampton N, Yokokawa M, Dryden D T F, Edwardson J M, Rao D N, Takeyasu K, Yoshimura S H and Henderson R M 2007 *Proc. Natl Acad. Sci. USA* **104** 12755
[20] Deer W A, Howie R A and Zussmann J 1992 *An Introduction to Rock-Forming Minerals* (Essex: Longman Group UK Limited)
[21] Erlandsson R, Hadziioannou G, Mate C M, McClelland G M and Chiang S 1988 *J. Chem. Phys.* **89** 5190